AUT Journal of Electrical Engineering

AUT J. Elec. Eng., 58(1) (2026) 205-224
DOI: 10.22060/eej.2025.24379.5697

Hybrid Energy System for EV Charging Station Using PV Fed Z-Source Modified Luo Converter and Fuel Cell Integration

Bollu Prabhakar[1,*], Dondapati Ravi Kishore[2], Uday kumar Upputuri[1], Sunkara Satya Suresh[1], Vallbhuni Govind[1]

[1] Department of Electrical and Electronics Engineering, Godavari Institute of Engineering and Technology (A), Rajahmundry, India.
[2] Department of Electrical and Electronics Engineering, Godavari Global University, Rajahmundry, India.

ABSTRACT: Petroleum-based vehicles are rapidly being phased out of the transportation sector as number of Electric Vehicles (EVs) rises. Nonetheless, the timely and well-coordinated growth of EV Charging Stations (CSs) is crucial for the quick implementation of EVs. Since a randomly distributed Photovoltaic (PV) system causes high power losses and voltage variances that exceed permitted limitations, integrating EVCSs into the current distribution network is difficult. This research proposes an EV charging solution supported by PV systems and fuel cells (FC) to sustain a variable load under an optimized energy management strategy. To overcome the intermittent nature of PV system, a Z-source modified Luo converter is employed, which provides higher efficiency and voltage gain. A Walrus optimized Proportional Integral (PI) controller is utilized to improve performance of developed converter with stabilized voltage. The performance of developed FC system is improved by using Boost converter with PI controller. In order to meet load requirement of the grid-connected charging station during unavailability of PV or FC shutdown condition, the grid source power the EV, thus ensures effective EV charging even under uncertain environmental conditions. The developed work is verified through MATLAB/Simulink and outcomes reveal higher converter efficieny of 97.14% with improved voltage gain, offering uninterrupted power supply to EVs.

Review History:
Received: Jul. 10, 2025
Revised: Nov. 10, 2025
Accepted: Dec. 02, 2025
Available Online: Jan. 10, 2026

Keywords:
Electric Vehicles
EVCSs
PV System
Z-source Modified Luo Converter
Walrus Optimized PI Controller

1- Introduction

The rise in the world's need for power has prompted the utilization of fossil fuel reserves and negatively impacted environmental situations, ultimately leading to global warming. With zero tailpipe emissions, EVs are now regarded as one of the most efficient forms of transportation [1-4]. However, EVs can't directly utilize fossil fuel resources; rather, their indirect fossil fuel consumption is increased by the energy derived from the system that distributes fossil fuels. Furthermore, EVs can only be maintainable while the electrical energy necessary for charging is developed from RES [5-8]. Microgrids are a means of achieving consistent and dependable power generation through the use of renewable energy [9, 10]. Among all the RES that is incorporated into the CS system, the PV source is acknowledged as one of the most practical options [11-13]. Regarding the increased need for fast charging during the day, the quick growth of PV generation maximizes power usage during peak hours by providing sufficient daytime generation. One practical way to support more clean energy, lower carbon emissions, and lessen the demand on the local grid for electricity is to directly integrate a PV system with EV charging stations [14,15]. Because Renewable Energy Sources (RESs), especially PV is intermittent, DC-DC converters need to be employed to stabilize the power output fluctuations [16]. In [17] Boost converter is developed that increases the input voltage to a higher output voltage. However, it produces significant output voltage ripple, requiring an additional filter to guarantee a smooth output. According to its design, the SEPIC converter [18, 19] operates in boost or buck mode by utilizing the PV system's maximum power. However, at greater duty ratios, the SEPIC converter is no longer able to generate a substantial voltage gain. In [20], the Luo converter is demonstrated, offering impressive features including increased voltage gain, less component count, minimal capacitor stress, and low voltage stress on power switches. However, the voltage stress on the switches of the converter is not equal to the output voltage. In [21] Z-source converter is developed that steps up and down the voltage, providing greater flexibility. Nevertheless, extra components are required for the Z-network, which improve the complexity and cost of the overall system. Therefore, a Z-source modified Luo converter is developed for improving the voltage in this paper.

PI controllers are employed for enhancing the grid-connected PV system's transient stability, and several

*Corresponding author's email: bolluprabhakar237@gmail.com

Copyrights for this article are retained by the author(s) with publishing rights granted to Amirkabir University Press. The content of this article is subject to the terms and conditions of the Creative Commons Attribution 4.0 International (CC-BY-NC 4.0) License. For more information, please visit https://www.creativecommons.org/licenses/by-nc/4.0/legalcode.

optimization approaches are used for the best possible tuning of PI control parameters. The literature [22] presents that Particle Swarm Optimization (PSO) is comparatively simpler than other optimization methods. PSO is good at avoiding local optima and investigating the global search space. The initial placements of the particles have a significant impact on PSO performance; incorrect initial positions might result in more iterations and longer convergence periods. The harmony search method, which was developed in [23], has a more robust convergence when it comes to the accuracy and efficiency of the solution while optimizing objective functions. Nevertheless, if the optimization algorithm concentrates on exploration, it will converge very slowly. Better performance is assured with optimal PI controller tuning; these optimization procedures frequently have lengthy execution times and are complex. An Artificial Bee Colony optimized PI Controller is developed in [24], which has less settling time. However, the computational complexity and the requirement for quick convergence make the implementation of ABC-optimized PI controllers difficult. In [25] Cuckoo search optimization algorithm is presented, which has strong global search capabilities, which helps in finding the optimal PI controller parameters. However, there is a risk of premature convergence, where the algorithm get trapped in a local optimum rather than predicting the global best solution. To overcome the above mentioned problems, this work develops a Walrus optimization algorithm for refining PI controller efficiency.

Energy Management System (EMS):

Seamless power is supplied to the EV system by the integration of dynamic EMS that regulates the coordinated operation of PV, FC, battery, and grid source. The EMS maximizes the use of RES by extracting power from the PV system if solar irradiance is adequate. In the absence of a PV system, FC is turned ON to provide supplemental power through a PI-controlled Boost converter. If both PV and FC are inadequate, the grid system charges the EV battery effectively.

The objectives of this paper are,

- Utilization of Z-source modified Luo converter for boosting PV system voltage for EV charging stations.
- For controlling the output of the developed converter Walrus optimized PI controller is exploited.
- For supplying an extra power supply to an EV battery, the fuel cell is employed with a boost converter.
- The battery with a bidirectional converter is exploited to provide a continuous supply to Evs.
- For control of bidirectional converter the ANN controller is employed on load side.

2- Proposed Methodology

The developed PV-Fuel cell-based EV charging stations is illustrated in Fig. 1. Normally, the output voltage of the PV system is low owing to variation in sunlight conditions. To

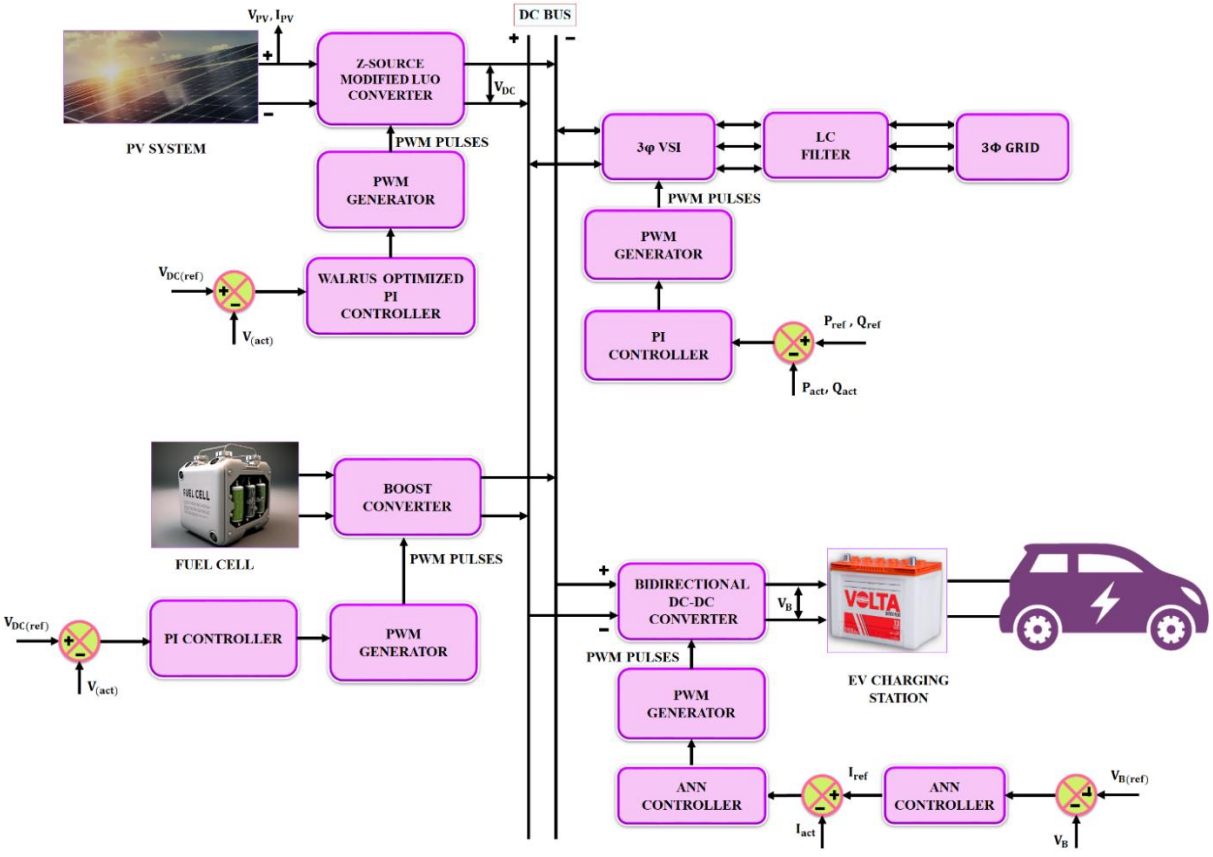

Fig. 1. PV-FC based EVCS.

maximize the PV system's low voltage, a Z-source modified Luo converter is employed that improves the efficiency of the overall system. Meanwhile, the converter's output is unstable, which is controlled through the implementation of Walrus-tuned PI control method that provides the stabilized power. Also, the Fuel cell acts as another resource and its low voltage is enhanced by a boost converter in which a PI controller is used to control it. Then, the 3ϕVSI is used to convert the DC supply into AC, which is also regulated by PI controller, and PWM generator is exploited to improve the inverter's functionality, guaranteeing low-distortion and high-quality AC power. The power supply is passed to 3ϕ grid through LC filter that removes unwanted noise and harmonics presented in the supply. The inverter enables grid-connected operation, allowing bidirectional power exchange and synchronization with the utility grid. This setup supports microgrid functionality, also as a stabilizing and supplementary source during dynamic load conditions.

Subsequently, additional energy from both PV and FC systems is given to the grid system while the bidirectional converter performs charging and discharging operation based on the need of the converter, in which its function is regulated by an ANN controller, thereby delivers consistent power supply to EVs.

2- 1- PV system

To create solar panels, many PV cells are linked in parallel or series. In a parallel design, the current rises while the voltage remains stable, but in a series configuration, the voltage increases while the current remains constant. N_p and N_S represent the total number of solar cells attached in shunt and series. The total photocurrent is the result of solar irradiation and cell temperature. Fig. 2 displays the single diode circuit diagram for the PV system.

The output voltage and current is related as,

$$I_{PV} = I_{ph} - I_O\left[e^{\frac{q(V_{PV}+I_{PV}R_S)}{N_S knT}-1}\right] - \frac{V_{PV}+I_{PV}R_S}{R_{sh}} \quad (1)$$

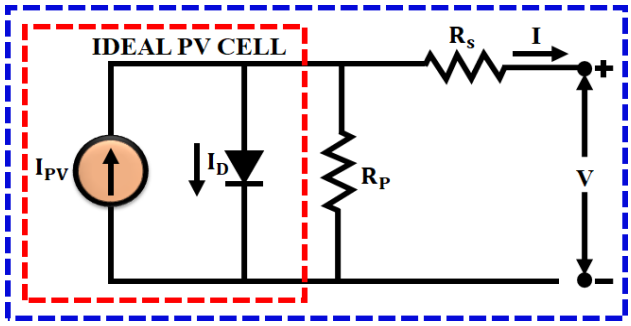

Fig. 2. Circuit of PV model.

Parameter n denotes ideality factor of the PV cell, while k represents Boltzmann's constant ($k = 1.3806\times10-23J/K$), and T is operating temperature of PV cell. Resistances R_S and R_{Sh} correspond to series and shunt resistances, respectively. V_{PV} and I_{PV} indicate output voltage and current of PV module. Symbol q refers to elementary charge of an electron, and I_O is reverse saturation current. To overcome inherently low voltage output of PV system, a Z-source modified Luo converter is utilized to effectively boost the voltage level.

2- 2- Z-Source Modified Luo Converter

A Z-source modified Luo converter is similar to that of a switching mode boost converter in behavior. The output DC voltage of this step-up power converter is higher than the input. With a relatively smaller number of components, it has a high gain. When attached in a cascade, this gain rises arithmetically step by step. The positive output Z-source modified Luo converter is shown in Fig. 3. This converter includes of input voltage (V_{PV}), input inductor L_1, capacitors $(C_1, C_2 \text{ and } C_3)$, switch S, diodes $(D_1 \text{and } D_2)$, inductors $(L_2 \text{and} L_3)$ output capacitor (C_O), output resistor (R_O) and output voltage (V_O).

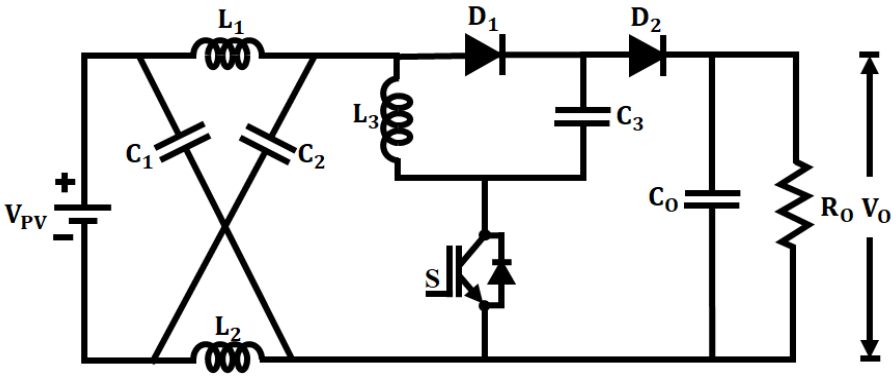

Fig. 3. Proposed converter.

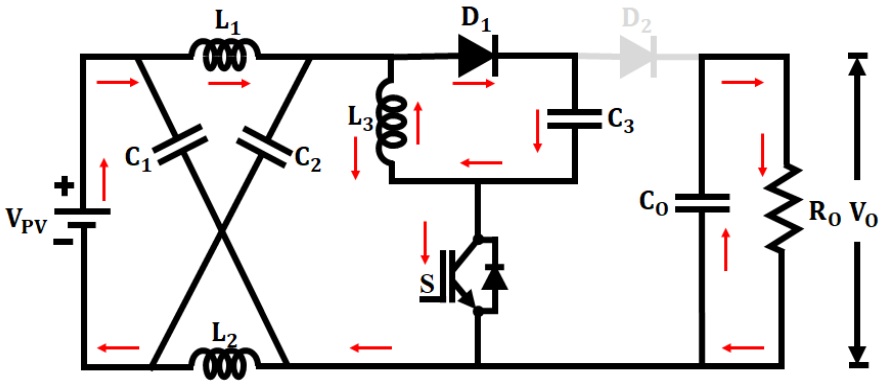

Fig. 4. Mode 1 of developed converter.

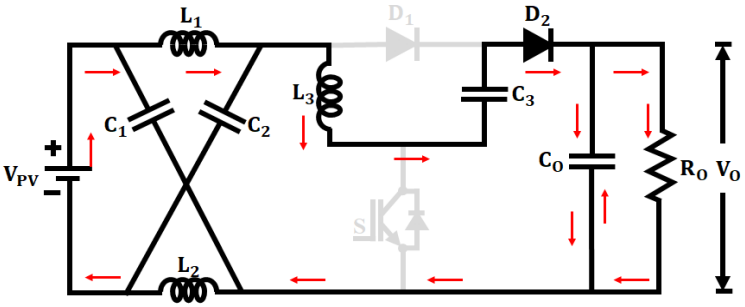

Fig. 5. Mode 2 of developed converter.

2- 2- 1- Mode 1

In this operating mode, switch S is turned ON, resulting in charging of inductor L_3 and simultaneous discharge of capacitor C_3, as shown in Fig. 4. Diode D_1 conducts forward, though a diode D_2 remains reverse biased, leading to discharge of the output capacitor C_O. During this phase, input section is electrically decoupled from load. Inductors $L_1 and\ L_2$ accumulate energy, while capacitors $C_1 and\ C_2$ release their stored charge. Applying Kirchhoff's Voltage Law (KVL), following relationships are established:

$$V_{PV} - V_{C1} - V_{L2} = 0 \tag{2}$$

$$V_{PV} - V_{L1} - V_{C2} = 0 \tag{3}$$

$$V_{L3} - V_{C3} = 0 \tag{4}$$

$$V_{CO} = V_O \tag{5}$$

2- 2- 2- Mode 2

In this mode, switch S is OFF, thereby inductor L_3 is discharged, making the capacitor C_3 charge. Here, the diode D_1 is reverse biased, D_2 is forward-biased and a capacitor C_O is charged. Inductors $L_1 and\ L_2$ are discharged and capacitors $C_1 and\ C_2$ are charged, as depicted in Fig. 5.

$$V_{L2} - V_{C2} - V_{L3} - V_{C3} - V_{CO} = 0 \tag{6}$$

$$V_{C1} - V_{L1} - V_{L3} - V_{C3} - V_{CO} = 0 \tag{7}$$

Subtracting equation (6) from (5)

$$V_{L2} - V_{C2} - V_{C1} - V_{L1} = 0 \tag{8}$$

Fig. 6 represents the timing diagram of the proposed converter, and its voltage gain is computed as,

$$\frac{V_o}{V_{in}} = \frac{2-k}{1-k} \tag{9}$$

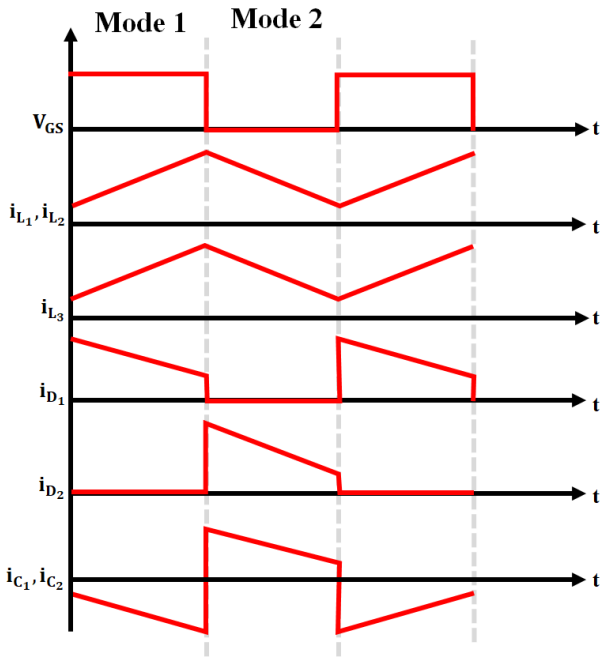

Fig. 6. Waveform of the developed converter.

Here, k represents the duty ratio of the switching signal applied to the main switch S, defined as:

$$k = \frac{t_{ON}}{T} \tag{10}$$

Where, t_{ON} is the time duration in which switch S is in the ON state, T is the total switching period. Then, the function of the converter is managed by a walrus optimized PI controller, which continued voltage of PV system.

2- 3- Walrus Optimized PI Controller

The Walrus optimized PI controller incorporates the Walrus optimization algorithm into the PI controller design. For optimal control performance, this method leverages the unique behaviours of the walrus to improve the process of tuning. This algorithm is inspired by the behavioural and social patterns of walruses.

2- 3- 1- Feeding strategy

The food is searched by the strongest walrus, similar to detecting an optimal solution in a search space. Walruses migrate to rocky beaches, indicating the exploration of distinct search areas for better solutions. To refine candidate solutions, these behaviors simulate local exploitation. Arbitrarily initialize a walrus's population, each indicating a candidate solution for PI controller parameters, such as proportional gain $\left(K_{p,i}\right)$ and integral gain $\left(K_{i,i}\right)$.

$$X = \begin{bmatrix} X_1 \\ X_2 \\ \vdots \\ X_N \end{bmatrix} \tag{11}$$

Where $X_i = \left[K_{p,i}, K_{i,i}\right]$ for the i^{th} walrus. For each walrus, the objective function is related to performance metrics like the Integral of Squared Error (ISE).

$$F_i = \int_0^T e^2(t)dt \tag{12}$$

Where the error signal between the actual and desired output is denoted as $e(t)$. The optimization aim for tweaking PI controller parameters is specified as minimizing the Integral of Squared Error (ISE) stated in Eq. (12). To produce balanced transient and steady-state responses, further performance weighting terms are incorporated.

$$J = \int_0^T \left(w_1 e^2(t) + w_2 e^2(t)\right)dt \tag{13}$$

Here w_1 and w_2 denote the relative weights of error magnitude and rate of change, respectively. The tuning ranges of K_p and integral gain K_i are limited to [0,5] and [0,0.05] respectively, maintaining system stability and limiting excessive overshoot. The WaOA algorithm iteratively adjusts these gains to reduce J, resulting in ideal control settings with the lowest ISE and smoothest voltage regulation.

Phase 1: Feeding strategy (Exploration)

Walruses graze by grazing on the sea floor and using their sensitive vibrissae and forceful flipper motions to identify food. Benthic bivalve mollusks, particularly clams, are preferred by walruses. As tgroup searches for food, the walrus with the tallest tusks and strongest physique takes lead. The proposed solution with highest objective function value is the group's smartest walrus. WaOA's ability to explore in global search is improved by Walruse's search behavior, which produces results in many scanning regions of search space. A new position is created as

$$X_i^{Pl} = X_i + rand_{i,j} . (X_{SW} - X_i). I_{i,j} \tag{14}$$

Where a random integer (1 or 2) is denoted by $I_{i,j}$ The strongest walrus's position is indicated by X_{SW}. The position is updated as,

$$\text{If } F_i^{P1} < F_i \text{ then } X_i = X_i^{P1} \tag{15}$$

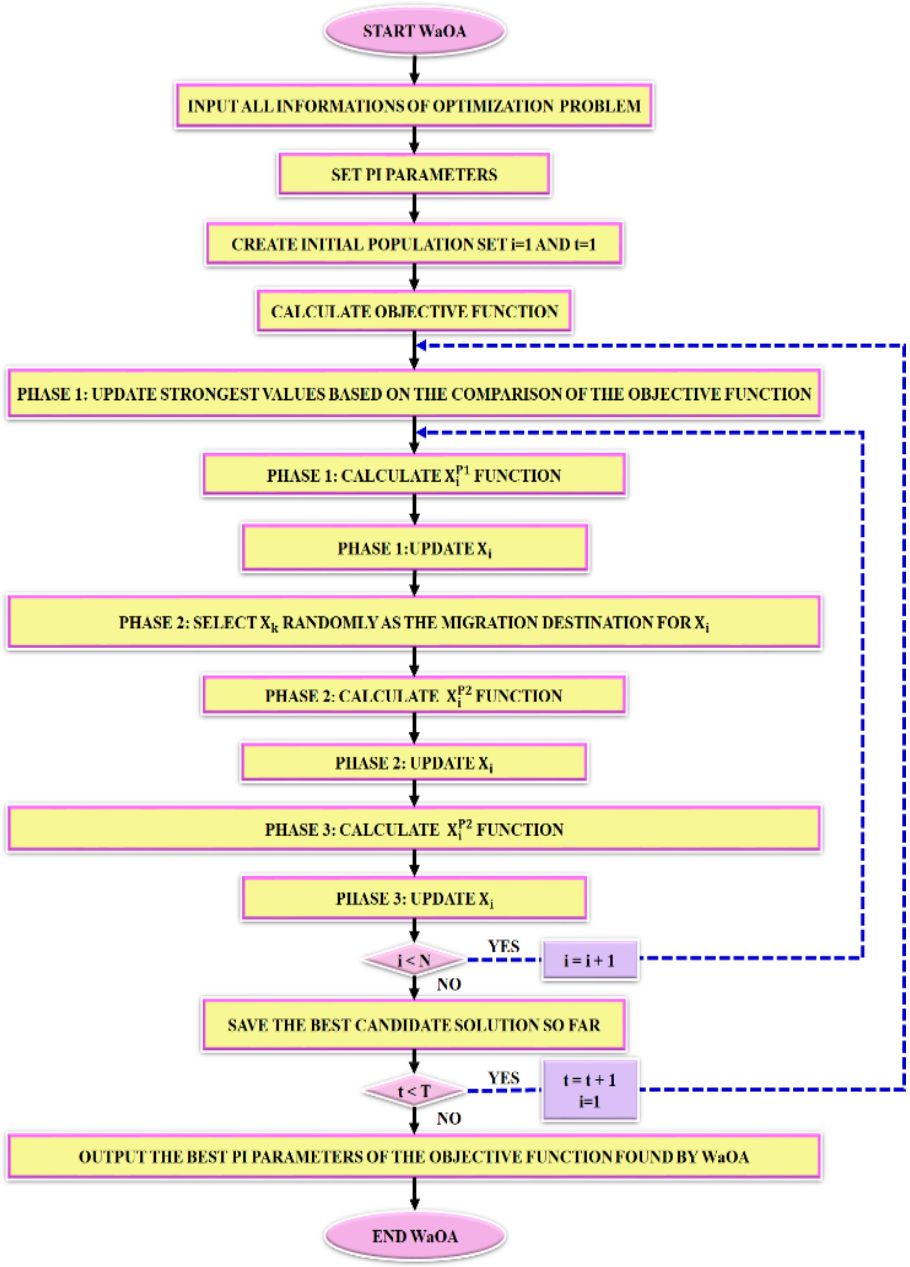

Fig. 7. Flowchart of Walrus optimized PI controller.

Phase 2: Relocating

One of walruses' typical behaviours is to migrate to rocky beaches due to late-summer air warming. This migratory strategy is used by WaOA to assist walruses in locating suitable spots inside search space. A new position is created as

$$X_i^{P2} = \frac{1}{N-1}\sum_{k=1,k\neq i}^{N} X_K \tag{16}$$

Fig.7. shows the flowchart of proposed Walrus optimized PI controller. The position is updated as,

$$\text{If } F_i^{P2} < F_i \text{then } X_i = X_i^{P2} \tag{17}$$

Phase 3: Exploitation

The killer whale and polar bear are constant threats to walruses. By mimicking this walrus's natural behavior, WaOA's exploitation capability in local search in the problem-solving space around possible solutions is increased. A new position in local neighborhood is generated as,

$$X_i^{P3} = X_i + rand_{i,j} \cdot \left(ub_j^{local} - lb_j^{local}\right) \tag{18}$$

Where jth variable's local bounds are indicated by ub_j^{local} and lb_j^{local}.

The position is updated as,

$$\text{If } F_i^{P3} < F_i \text{ then } X_i = X_i^{P3} \tag{19}$$

2- 3- 2- Iteration process

The first WaOA iteration is finished when the walruses' position has been updated based on the phases' implementation. New values are then computed for the walruses' position and the objective functions. Using the WaOA procedures as a guide, candidate solutions are updated and improved. Until a stopping condition is satisfied, repeat steps two and three.

2- 3- 3- Final solution

WaOA presents the optimal candidate solution discovered during algorithm execution as a solution to the specified problem when algorithm has finished running. Return the best candidate solution as the PI controller's optimal parameters

$$X_{best} = \arg\min F_i \tag{20}$$

The objective function value amid all walruses is denoted by F_i.

Fig. 8. Displays convergence curve of proposed optimized controller. Based on the execution of the WaOA, optimal proportional gain (K□) and integral gain (K_i) for the developed converter were found to be K□ = 2.35 and K_i = 0.015. These values yielded the lowest Integral of Squared Error (ISE) and ensured rapid transient response with minimal overshoot and steady-state error.

By simulating walrus behaviours, walrus optimized PI controller attains a balance between exploration and exploitation, leading to optimal solutions. Another RES is a fuel cell, and its voltage is improved by a boost converter.

2- 4- Fuel Cell-Fed Boost Converter

A fuel cell is an energy transformation device that directly transforms chemical reactions into electrical energy with some heat, while producing water as a by-product. where $VFC\ and\ IFC$ are the voltage and current of the fuel cell, R_W is the resistance coefficient, R_{act} stands actual value of the resistance, E_{Nernst} is the output voltage of each component, and R_{con} is the resistance concentration loss. An important component of an FC regulator is the excess ratio of oxygen, or λ_o. Equations (21) and (22) each provide an independent description of the necessary stack current I_st.

$$W_{H2,reac} = 2M_{H2}\,(nI_{st}/4F) \tag{21}$$

$$W_{O2,reac} = 2M_{O2}(nI_{st}/4F) \tag{22}$$

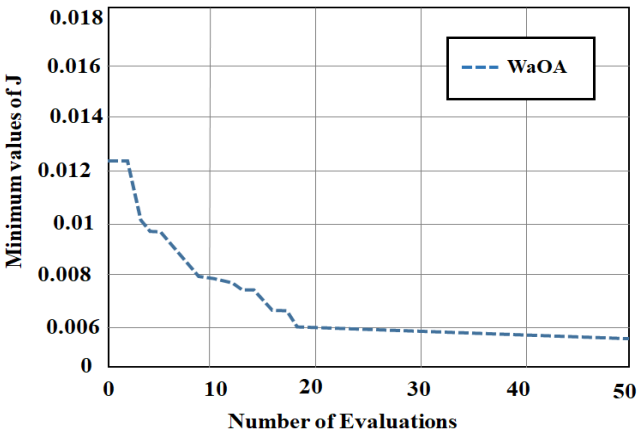

Fig. 8. Convergence curve of WaOA.

In this case, M_H stands for mass of hydrogen, M_o for mass of oxygen, F for the Faraday constant, and n for the number of cells. The movement of hydrogen is represented by $W_{H2,reac}$ and the stack is denoted by I_{st}. Equation (23) states that in order to meet the current demand, a connection between the flow of oxygen and the stack is required.

$$\lambda_{o2} = {W_{O2,ca,in}}/{W_{O2,reac}} \tag{23}$$

Equation (20) is the sole basis for the oxygen excess ratio, which is expressed as λ_{02}. Flow of oxygen disbursed is characterized by $W_{O2,reac}$, and the movement of cathode oxygen is shown by $W_{O2,ca,in}$. Equation (24) represents the steady-state equation:

$$V_{FC} = A - B.ln\left(1 + \frac{i_{FC}}{C}\right) - D.e^{\frac{i_{FC}}{E}} \tag{24}$$

Here $A, B, C, and\ D$ tuned parameters and the stack current of FC is expressed as I_{FC}. Fig. 9 depicts the traditional boost converter topology. Fig. 10 depicts the boost converter's two modes of operation. The boost converter, which is needed for low-to-medium power levels, is an easy and sufficient solution for applications where extremely high voltage step-up ratios are not required. The direct current input of the converter is powered by DC sources like fuel cells. In this system, the input voltage is raised by means of three primary components: an inductor, a diode, and a power switch. Boost converter's output is coupled to a capacitor that reduces and stabilizes output voltage fluctuations. Lastly, an output capacitor is connected to a load in the form of adjustable resistors.

In stage1, the switch S is active, causing an improvement

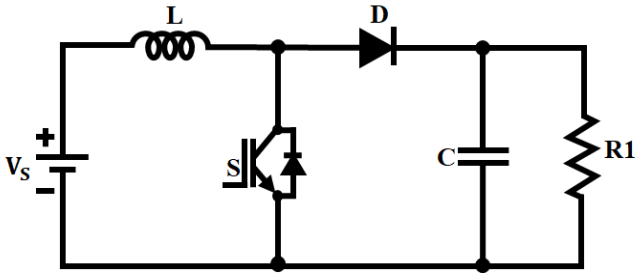

Fig. 9. Boost converter.

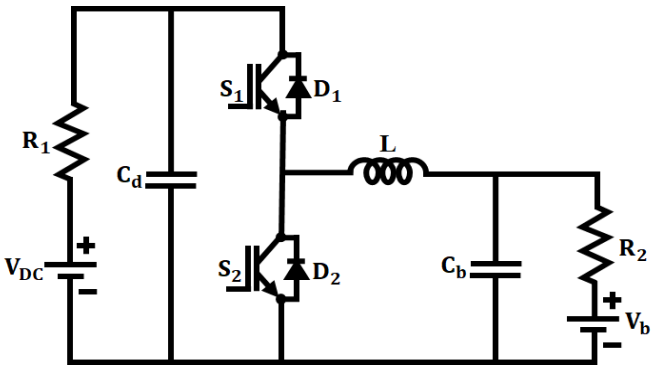

Fig. 11. Bidirectional converter.

in inductor current. In this stage, the expression becomes,

$$\Delta_{i\,lON} = \frac{DT}{L} V_S \tag{25}$$

In stage 2, switch S is inactive, the inductor current passes via load, and the expression becomes,

$$\Delta_{i\,lOFF} = \frac{(V_S - V_O)(1-D)T}{L} \tag{26}$$

By utilizing the CCM operation and the volt-second balance principle, the static gain is expressed as,

$$G_v = \frac{V_o}{V_i} = \frac{1}{1-D} \cdot \frac{1}{\left(1+(R_L/((1-D)^2.R_o))\right)} \tag{27}$$

Here, the fuel cell based Boost converter provides additional power to charge EVs. Also, the battery with a bidirectional converter is exploited for EV charging when there is no power available from HRES.

2- 5- Battery System with Bidirectional Converter

A bidirectional converter in the battery system depicted in Fig. 11 enables both power mode operation while the battery is being charged and regeneration mode operation when the battery is being discharged. Power transfers from the DC link to the battery during battery bank charging and back to DC link during battery bank discharge. When the inductor is charged, the diode D_2 reverse bias causes S_1 is in the OFF state and S_2 is in the ON state. When both switches are in ON state, the diode D_2 is forward-biased.

Similarly, when S_1 is in ON state and S_2 is in the OFF state during discharging, the inductor's current drops to zero and polarity charges. Diode D_1 turns forward bias when S_1 and S_2 are in the ON state. However, achieving a stable voltage requires an efficient controller, in which an ANN controller is exploited in this work to monitor the battery's state of charge.

2- 6- ANN Controller

Several factors that are pertinent to the control procedure are usually included in the input signals sent to an ANN controller for managing switching power signals from a battery bank. The proposed ANN controller employs a feed-forward neural network architecture with two hidden layers, each comprising 10 neurons. The sigmoid activation function is utilized in both hidden layers to ensure non-linear mapping, while the output layer integrates a linear activation function for generating precise switching control signals. The network is trained using the backpropagation algorithm with gradient descent optimization, ensuring convergence and adaptability to dynamic operating condition The Levenberg-Marquardt back propagation algorithm is applied, with a learning rate

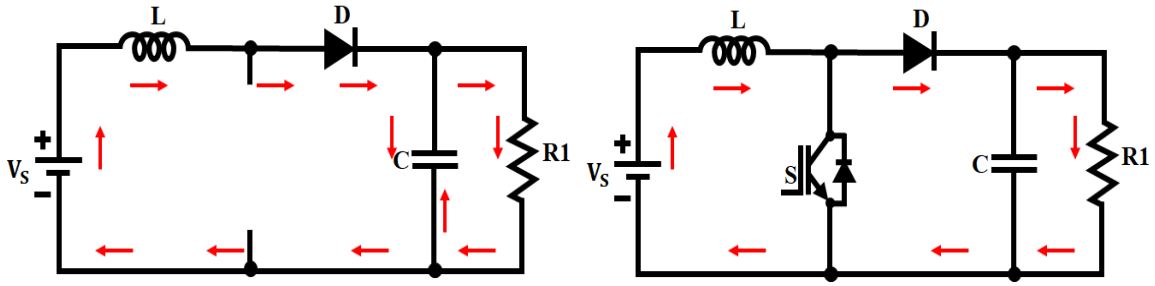

Fig. 10. Operating Modes of Boost converter.

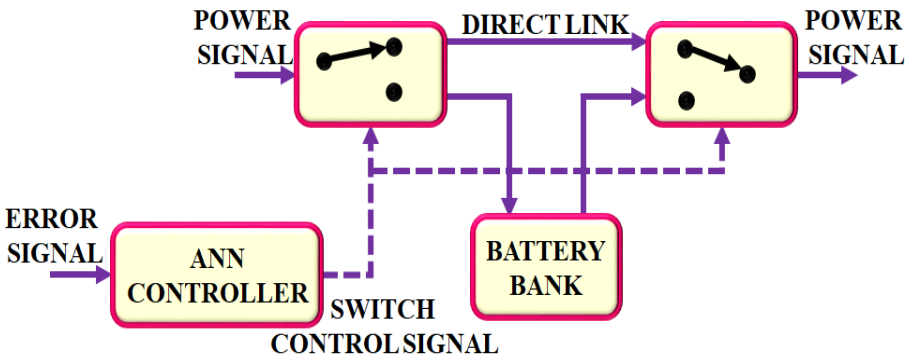

Fig. 12. Energy management using ANN controller.

of 0.01 and a momentum coefficient of 0.9.s. The input signals are battery voltage, current, SOC, temperature, load demand, and perhaps other pertinent factors. These inputs are normalized and fed into the ANN to evaluate the system's operational state. Switching control signals for power switches connected to the battery bank, determining ON/OFF states to optimize energy flow and maintain grid stability. The fundamental neuron model used in the ANN controller is,

$$\alpha = \left(\sum_{j=1}^{n} w_j u_j + \Phi\right) \tag{28}$$

Fig. 12 depicts the basic design of ANN controller. This ANN-assisted control approach enhances battery reliability, reduces switching losses, and ensures continuous grid support under varying load and environmental conditions.

3- Result and Discussions

Waveforms of the proposed hybrid energy system for EV charging stations are examined in this section. The proposed work is executed in MATLAB/Simulink, and its proficiency is demonstrated by comparison with traditional methods. Parameters specifications for the proposed research are specified in Table 1.

Fig. 13 system includes a solar Z-source modified Luo converter and a fuel cell boost converter, whose outputs are combined to power the DC link. A bidirectional battery converter controls charging and discharging operations, and surplus energy is released via a dump load. The three-phase inverter connects the DC link to the utility grid, allowing bidirectional power exchange while ensuring grid stability.

CASE 1: Constant temperature and intensity

Waveform for solar panel's properties under conditions of constant temperature and intensity is presented in Fig. 14. The system as a whole maintains the solar panel's temperature at a constant 35°C. Additionally, solar panel maintains a consistent intensity value of $1000W/m^2$ throughout the system. After that, solar panel's voltage is maintained throughout system at 230V. Also, output current of solar panel is initially varied and sustained at a value of $32A$ after an initial transient fluctuation of ±0.8 A. Based on these values, converter's output is varied, which is discussed below.

Waveform for the developed converter is represented in Fig. 15. The converter's output voltage is continuous at 600 V, with a maximum transient fluctuation of ±2 V (0.33%). At first, the converter's output current is varied and maintained to stable value of $10A$. Under constant environmental circumstances, indicate strong dynamic stability and quick voltage regulation.

The waveform for input and output power is indicated in Fig. 16. Input power fluctuates during the transient period before stabilizing at an average of 7000 W with a variance of ±90 W. The output power is stable at 6.8×10^3W, with slight variations within ±120 W.**Varying temperature and intensity**

The waveform of the solar panel in changing temperature and intensity is indicated in Fig. 17. When irradiance ranges from $800-1000W/m^2$ and the temperature ranges from $25-40°C$, the PV output voltage averages 230 V with ±3 V (1.3%) variations, and the current ranges from 8.5 A ± 0.25 A. These low-magnitude oscillations demonstrate that the control strategy efficiently reduces transient impacts induced by environmental changes.

Fig. 18 signifies proposed converter output voltage and output current waveform. Throughout the transient interval, the converter's output voltage rises and stabilizes at 600 V with a maximum variance of ±2.5 V (0.4%). The output current stabilizes at 10 A with oscillations of ±0.3 A during steady state. These findings show the converter's fast settling reaction and effective voltage regulation in dynamic operation situations.

Under variable temperature and intensity, the power waveforms are shown in Fig. 19. During the initial transients, the input power swings before settling at an average of 7000 W, with a variance of ±100 W (1.4%). The output power averages 6.8 × 10^4 W, with minor variations of ±150 W (2.2%). These findings demonstrate that the suggested converter maintains high power stability and little fluctuation

Table 1. Specification of parameters.

Parameter	Specification
PV System	
Rated Power	10kW
Open Circuit Voltage	37.25V
Short Circuit Current	8.95A
No. of Panels in Parallel	2
No. of Panels in series	21
Temperature	35 $°C$
Irradiance	1000 W/m^2
Z-source modified Luo Converter	
Switching frequency	10KHz
Input Voltage	230V
Output Voltage	600V
L_1, L_2, L_3	4.7mH
C_1, C_2, C_3	22µF
C_O	2200µF
Fuel cell	
Maximum Operating Point $[I_{end}(A)]$	33.2 A
Maximum Operating Point $[V_{end}(V)]$	104.86 V
No. of cells	119
Nominal supply pressure (Air[bar])	1 bar
Nominal composition (%) $[H_2, O_2 H_2 O]$	[50, 21, 3] %
Nominal Operating Point $[I_{nom}(A)]$	30 A
Nominal Operating Point $[V_{nom}(V)]$	106.5 V
Operating temperature (Celsius)	600 $°C$
Nominal Air flow (Ipm)	635 L min^{-1}
Nominal supply pressure (fuel[bar])	1.35 bar
Battery (Li-ion)	
SOC	90%
Nominal Voltage	60V

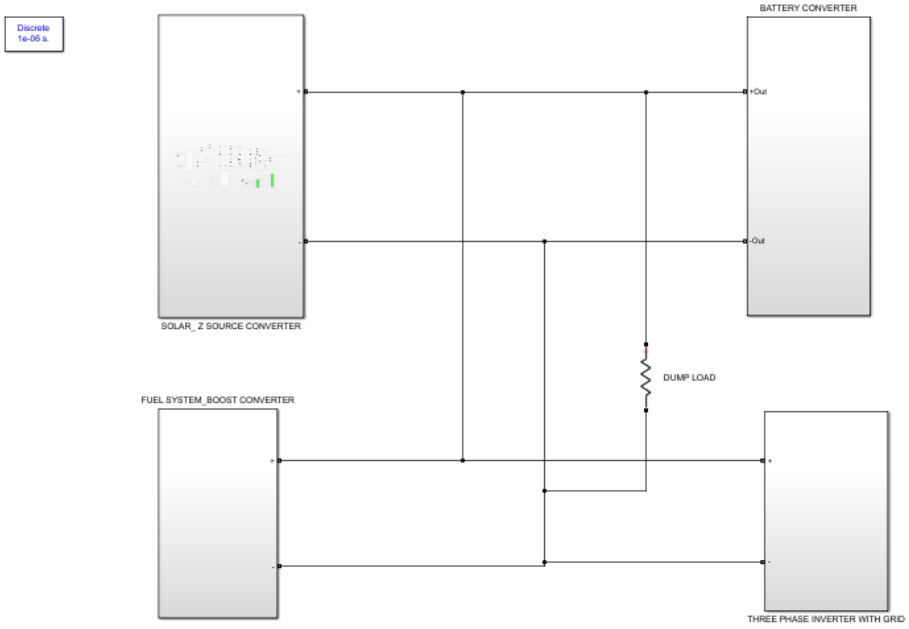

Fig. 13. Simulink model of proposed hybrid PV-Fuel Cell EV charging system.

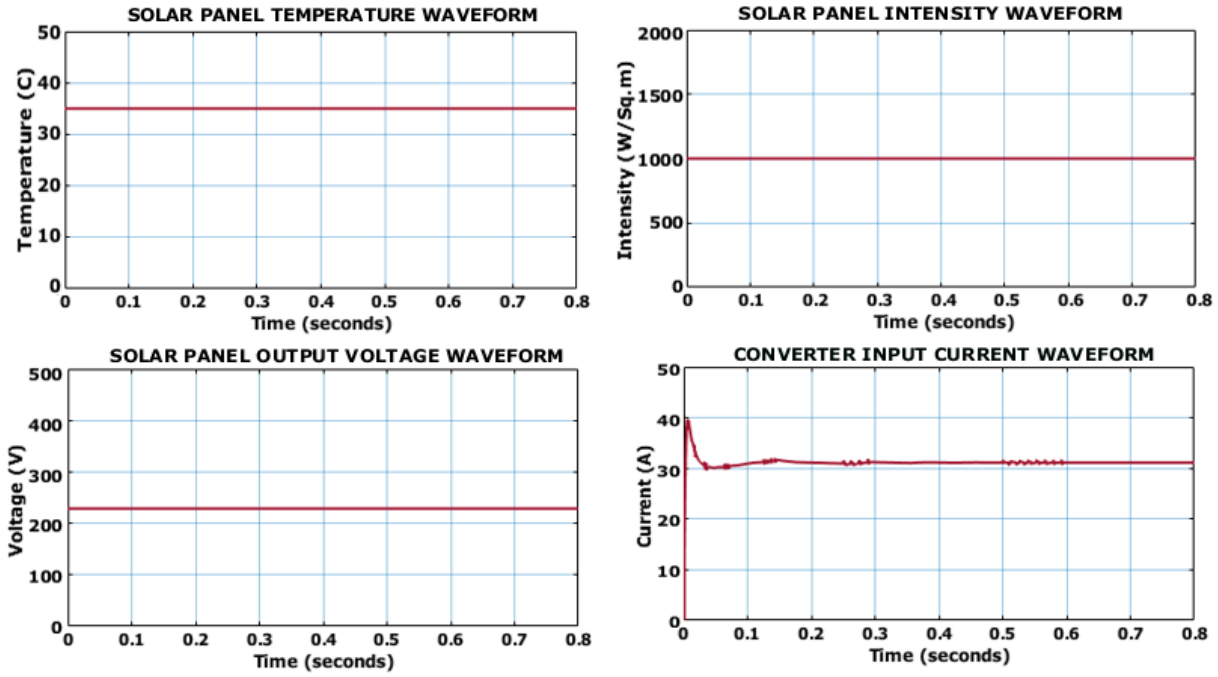

Fig. 14. PV panel waveforms.

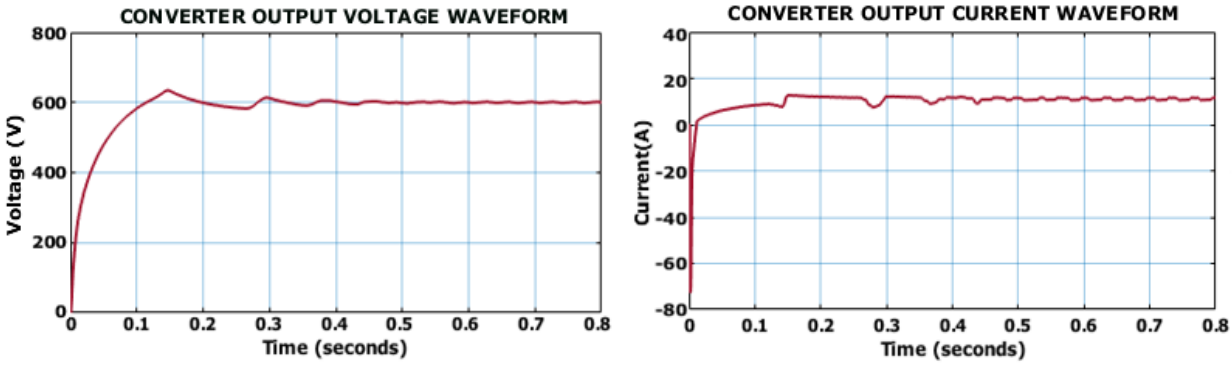

Fig. 15. Converter output waveform under case 1.

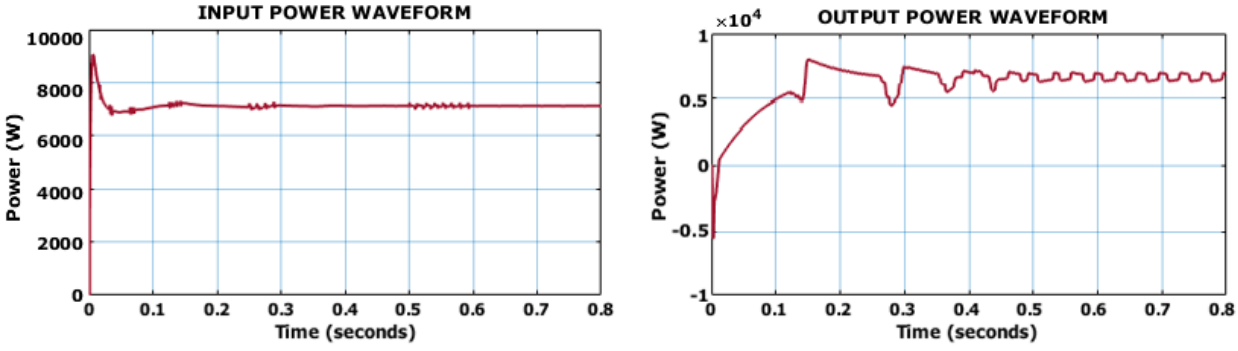

Fig. 16. Waveform of power at case 1.

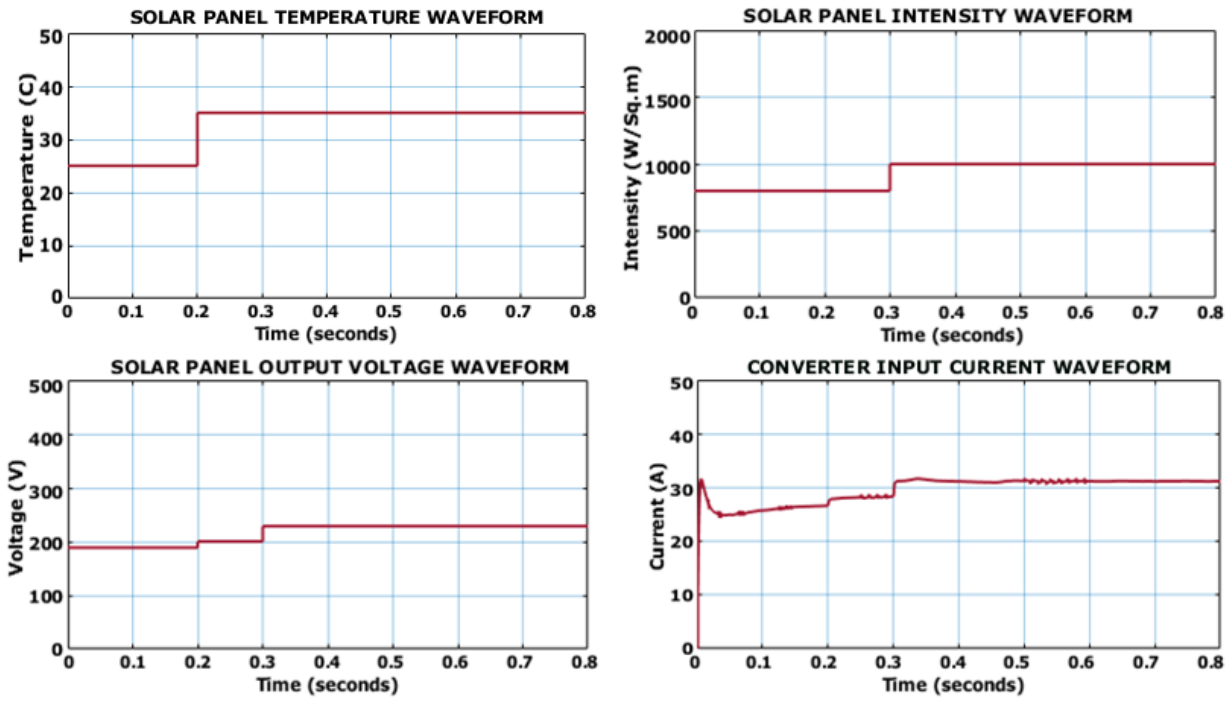

Fig. 17. PV system waveforms.

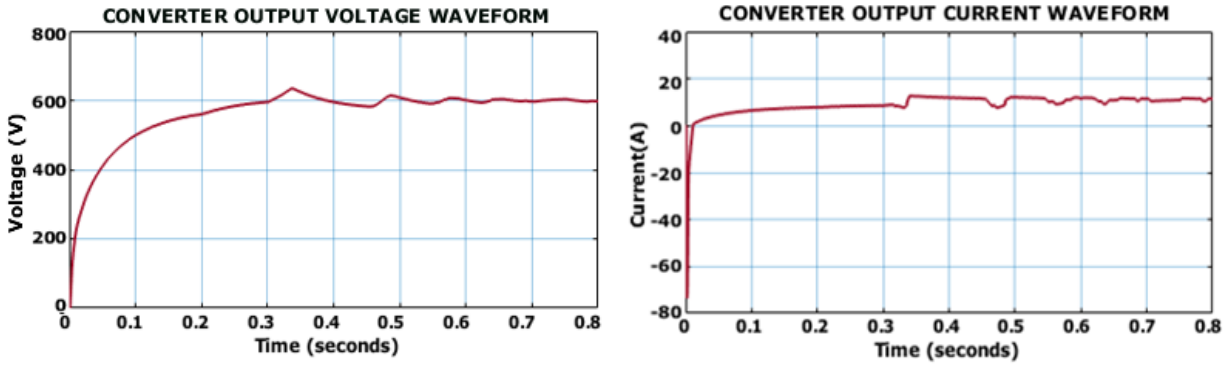

Fig. 18. Output waveform of proposed converter.

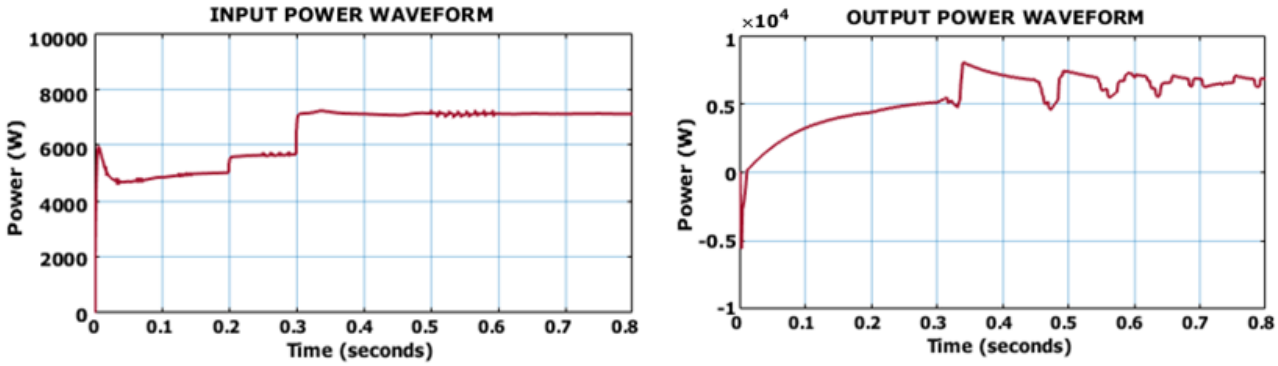

Fig. 19. Power Waveform at case 2.

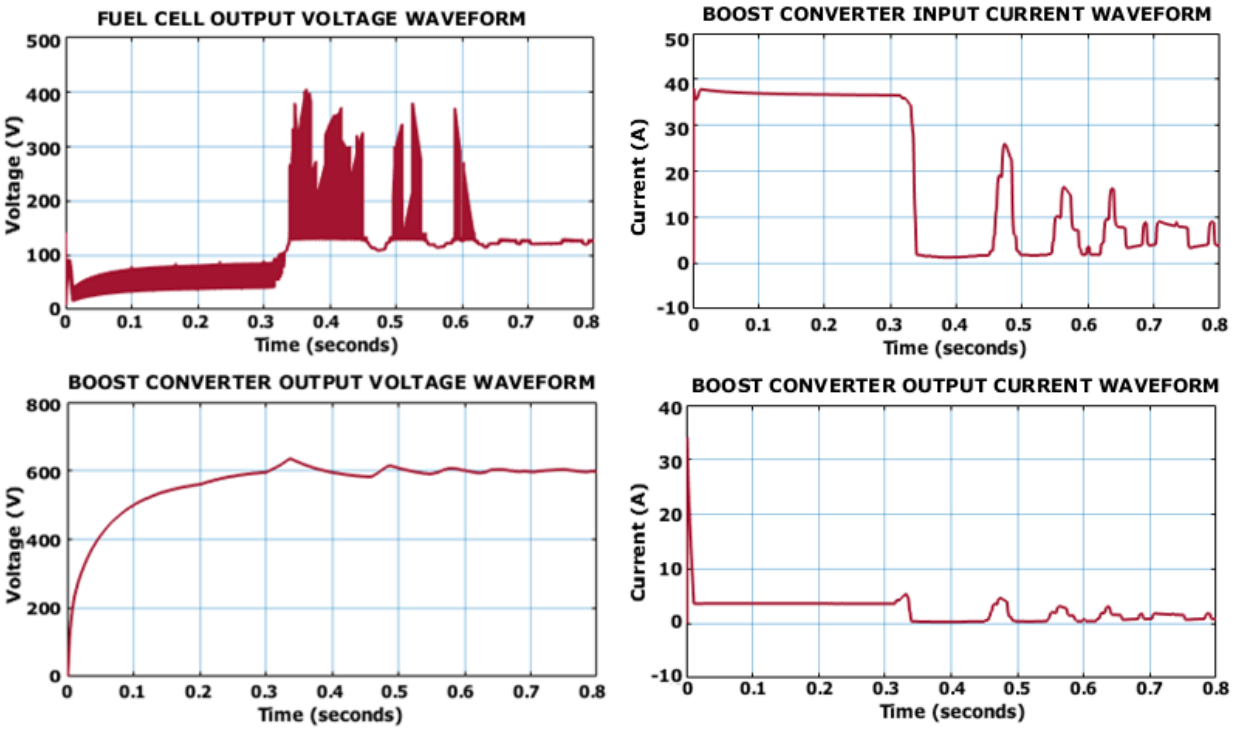

Fig. 20. Waveforms of Fuel Cell with Boost converter output.

despite dynamic environmental disturbances.

The outcomes of fuel cell with converter output is shown in Fig. 20. Initially, the fuel cell voltage fluctuates somewhat before settling at 110 V, with a variance of ±2 V. The boost converter's input current peaks during starting and stabilizes at 5 A, with fluctuations within ±0.15. Based on the fuel cell's input voltage, the output voltage is enhanced with a boost converter with the value of $600V$. Accordingly, the output current is stabilized in the beginning and finally has some fluctuations with a value of 2A.

The battery characteristics waveforms in Fig. 21 illustrate the effectiveness of the control strategy in regulation. The SOC waveform remains constant at 90% during the simulation period, ensuring that the battery is in a high state of charge and held in reserve for potential energy exchange. The current waveform shows an initial transient spike that peaks close to 40A, which is likely due to load fluctuation. After this transient period, the current stabilizes near 3A. Similarly, the voltage waveform remains steady at approximately 60 V over the entire duration, demonstrating effective voltage regulation by the ANN controller.

Fig. 22 indicates the waveform of the grid. The voltage of the grid is conserved a stable value of $350V$ during the entire period. Consequently, grid current continues to stable value of $12A$. Also, in-phase grid voltage and current is continued to the value of $350V$. It denotes that the current and voltage in the grid is controlled by PI controller to continue a stable and constant level. This confirms the grid-tied nature of the system, with stable voltage and current profiles indicating continuous synchronization and support from the grid, characteristic of a grid-connected microgrid. Real and reactive power waveforms are illustrated in Fig. 23. Reactive power consumption is decreased, which makes it possible to use active power in the system more effectively, which raises total power efficiency and improves real power performance.

Figure 24 shows that the converter maintains a consistent efficiency of 97.14% under constant and varying conditions. The overall converter efficiency is calculated using the MATLAB/Simulink model's total DC output power to total DC input power ratio. It is described as,

$$\eta = \frac{P_{out}}{P_{in}} \times 100$$

The average input voltage and current are represented by V_{in} and I_{in} , correspondingly. The Z-source modified Luo converter's output quantities are denoted by V_{out} and I_{out} . The average results were obtained once the system had reached steady-state functioning. The computed efficiency of 97.14% indicates the steady-state power conversion efficiency, which includes conduction and switching losses, as assessed using MATLAB/Simulink simulation data.The waveform of Total Harmonic Distortion (THD) spectra for R, Y, and B phases is illustrated in Fig. 25, showing respective

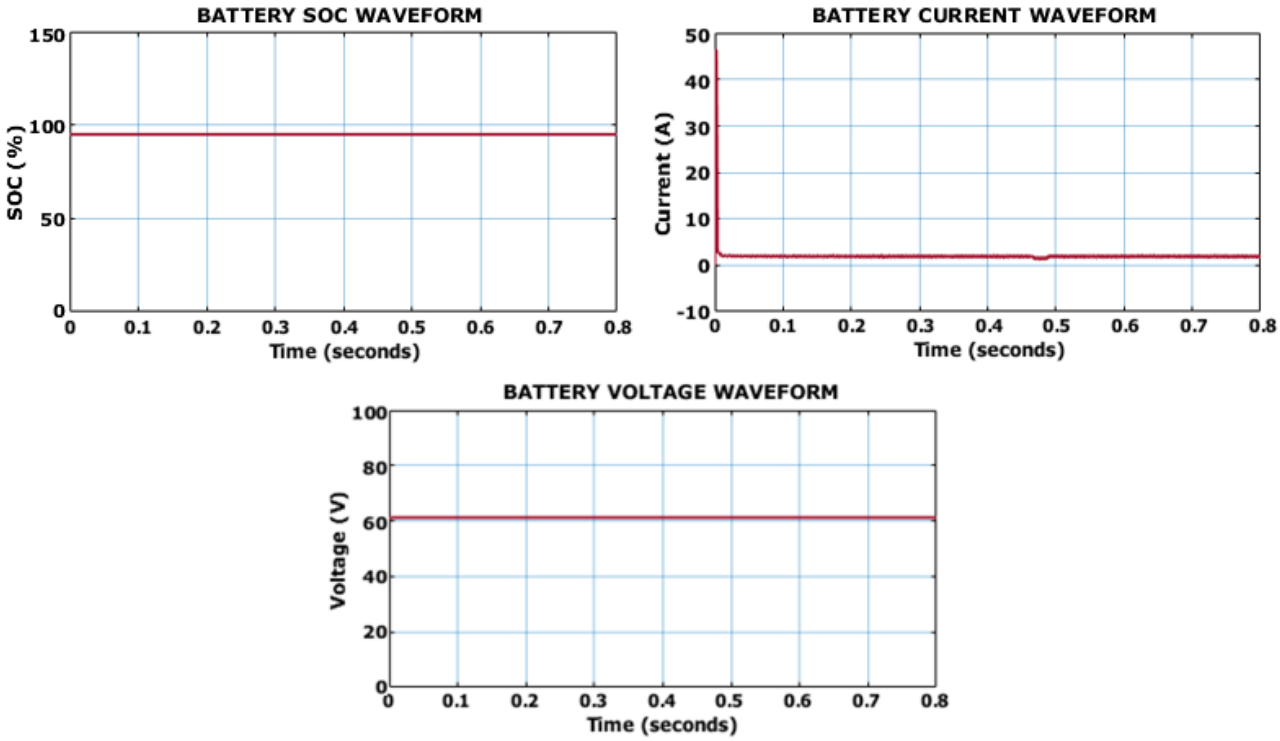

Fig. 21. Waveform of battery

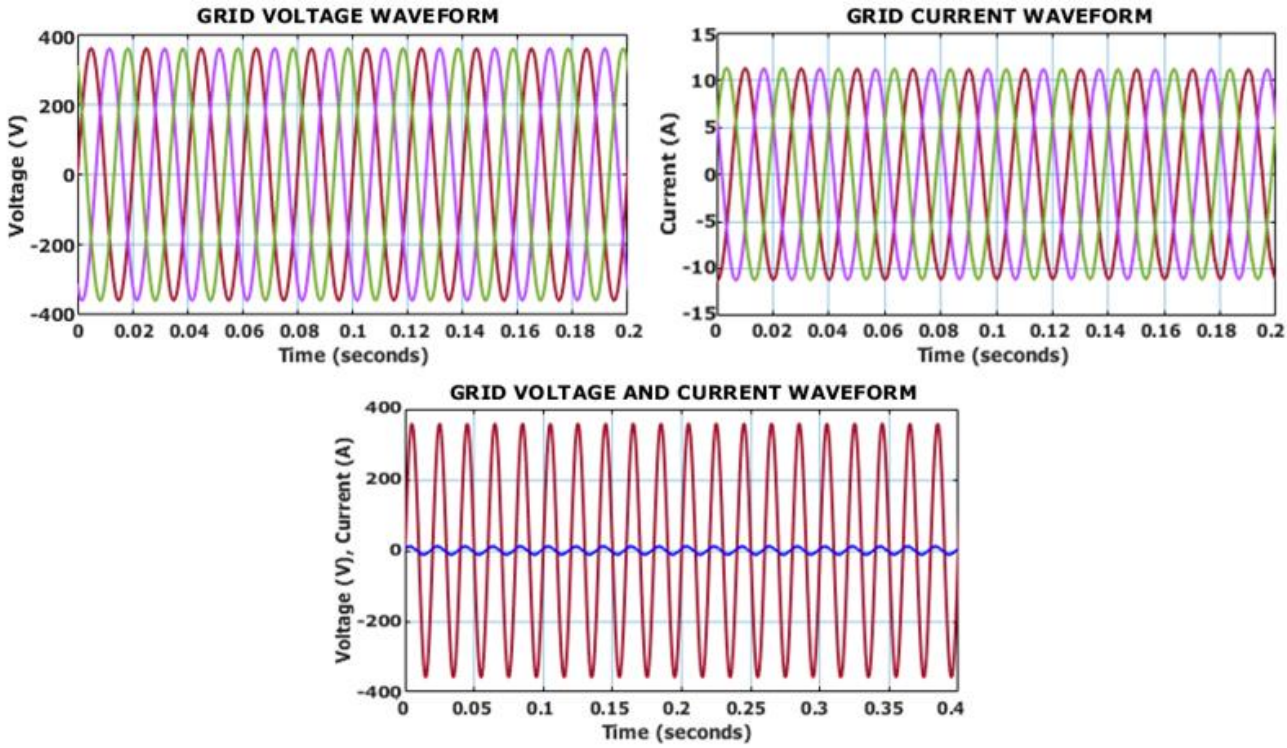

Fig. 22. Waveform of grid.

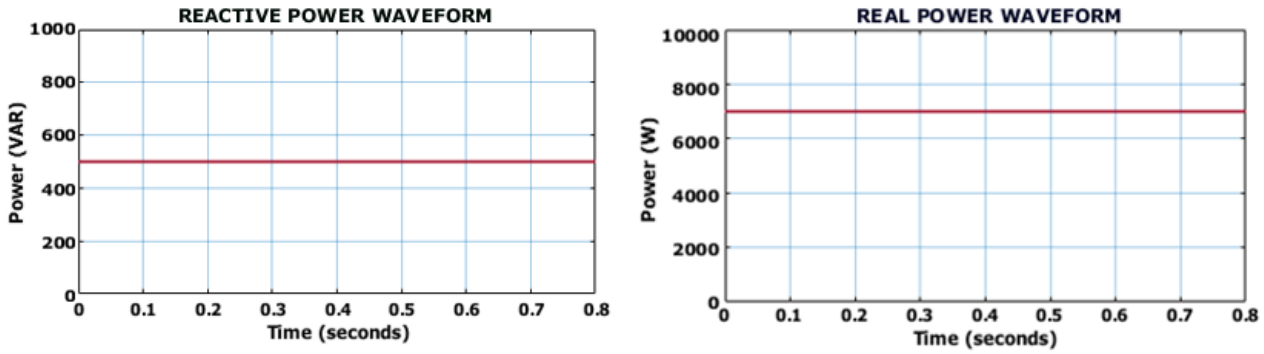

Fig. 23. Waveform of real and reactive power.

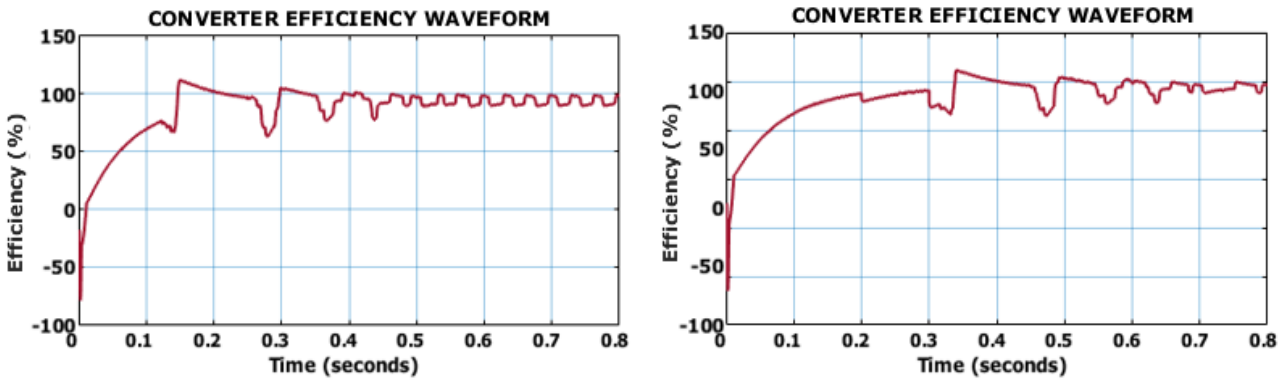

Fig. 24. Waveform of converter efficiency under constant and varying conditions.

THD values of 0.54%, 0.63%, and 0.43%. Among them, the B phase exhibits the lower distortion level, signifying better power quality compared to the R and Y phases.

Fig. 26. illustrates the comparative efficiency analysis of various converter topologies, such as High Step-Up Switched Z-Source Converter (HS-SZSC) [26], Trans-quasi-Z-source (TQZS) Boost [27], KY [28], Super-lift Luo and Boost Converter (SLBC) [29], SEPIC-Luo [30], and the proposed converter. The respective efficiency values recorded are 83.60%, 92%, 93%, 94.80%, 96%, and 97.14%. Among these, the proposed converter validates enhanced performance in efficiency, overtaking all existing designs. It clearly validates its superior energy conversion capability and optimized performance under the tested conditions.

Table 2 presents the comparative study of different converters with control approaches, highlighting their system configurations, peak efficiencies, voltage gain capabilities, input voltage, output power, and switching frequency. It demonstrates that the proposed converter with a walrus optimized PI controller outperforms existing designs by achieving the highest efficiency (97.14%) and voltage gain, while maintaining a compact architecture with minimal storage dependency.

Fig. 27 illustrates the analysis of voltage gain for bidirectional DC-DC [31], wide voltage gain [32], and the developed converter. The proposed converter has highest voltage gain among conventional converters, indicating its maximum efficiency. The voltage stress between bidirectional DC-DC [31], wide voltage gain [32], and the proposed converter is shown in Fig. 28, it has lesser voltage stress than existing converter topologies, which enhances converter efficiency.

To ensure an impartial assessment of performance, the PSO-PI and GWO-PI controllers are developed in MATLAB/ Simulink under similar converter and load conditions. The controller parameters and tuning approaches are taken from [33] and [34], respectively, and used the standard gain selection and convergence settings. These reference models offer valid baseline performance indicators for testing the proposed Walrus-optimized PI controller's settling and rising times.

Table 3 represents the analysis of optimized-PI controllers for PSO [33], GWO [34] and the developed algorithm. The settling time for developed Walrus optimized PI controller is 0.00089 s, which is better than settling time of PSO-PI (0.0075s) and GWO-PI (0.00406s). Also, the rising time

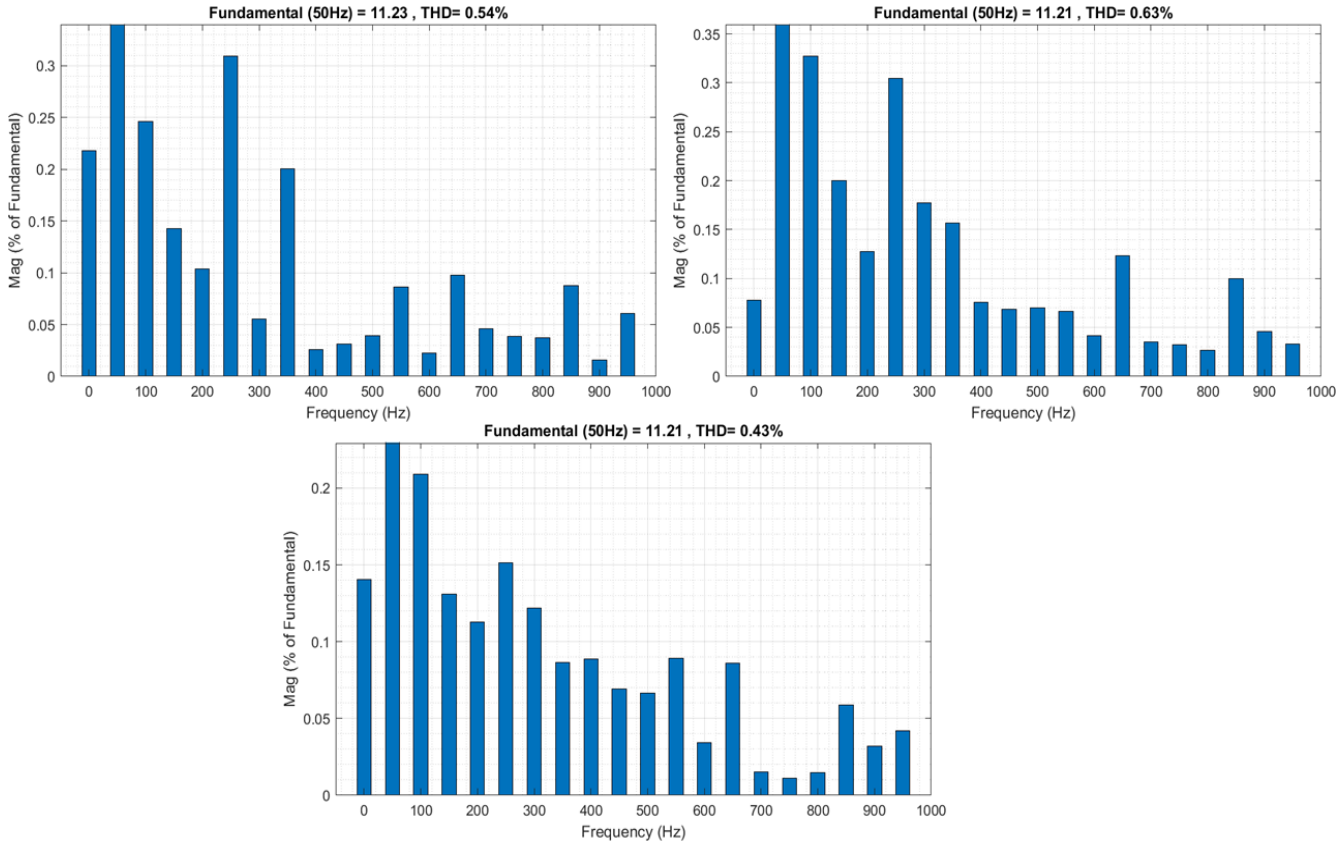

Fig. 25. Waveform of THD.

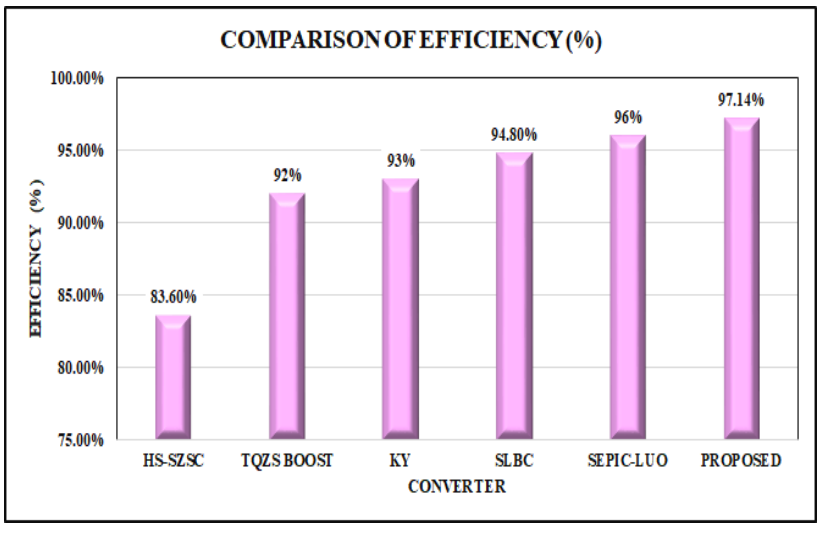

Fig. 26. Analysis of efficiency.

Table 2. Comparative analysis of converter with control topologies.

References	[26]	[30]	Proposed
System Components	PV, Grid.	PV, Wind, Grid, Battery, EV Load	PV, FC, Grid, Battery.
Converter Topology	HS-SZSC	SEPIC-Luo	Z-Source Modified Luo Converter
Control Algorithm	PI Controller	PI Controller	Walrus Optimized PI controller
Peak Efficiency (%)	83.60%,	96%	97.14%
Voltage Gain (G)	Moderate	High	Very High
Input Voltage (V)	**35V**	120V	230V
Output Power (W)	1200W	4500W	6800W
Switching Frequency (KHz)	30KHz	100KHz	10KHz

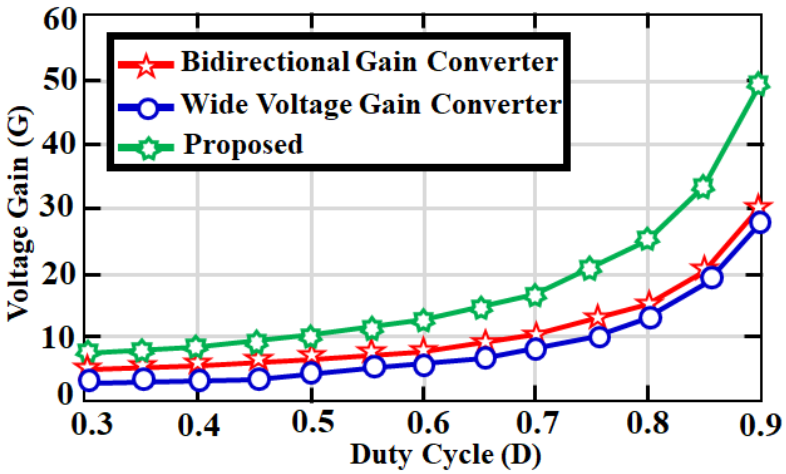

Fig. 27. Analysis of voltage gain.

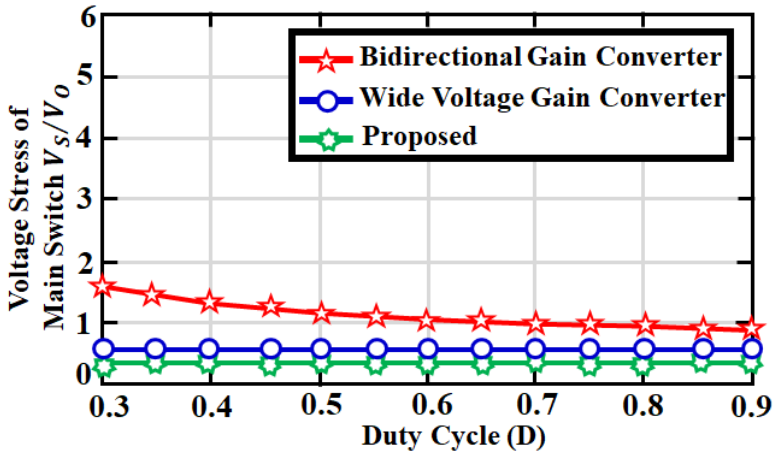

Fig. 28. Analysis of voltage stress on switch.

Table 3. Analysis of PI controllers.

Approaches	Settling Time (s)	Rising Time (s)
PSO-PI [33]	0.0075 s	0.00815 s
GWO-PI [34]	0.00406 s	0.000228 s
PROPOSED	0.00089 s	0.00013 s

for PSO-PI, GWO-PI, and developed method is 0.00815 s, 0.000228 s and 0.00013 s. The developed method attains the better performance interms of rising time than listed approaches.

4- Conclusion

This research develops a novel hybrid energy system for EV charging station using PV fed Z-source modified Luo converter and a fuel cell based Boost converter. The PV system's low voltage is enhanced by Z-source modified Luo converter with higher efficiency. Furthermore, the Walrus optimized PI controller manages the performance of converter with stabilized voltage. Also, the FC based Boost converter with PI controller is employed to charge the electric vehicles. The battery with bidirectional converter is exploited to provide continuous power supply to Evs in the necessary period. The overall research is implemented in MATLAB/ Simulink and outcomes demonstrate that developed method provides higher efficiency of 97.14%, ensures the constant power supply to EVs.

References

[1] B. Singh, A. Verma, A. Chandra, and K. Al-Haddad, "Implementation of solar PV-battery and diesel generator-based electric vehicle charging station", IEEE Transactions on Industry Applications, vol. 56, no. 4, pp. 4007 – 4016, 2020.

[2] D. S. Abraham, B. Chandrasekar, N. Rajamanickam, P. Vishnuram, V. Ramakrishnan, M. Bajaj, M. Piecha, V. Blazek, and L. Prokop, "Fuzzy-based efficient control of DC microgrid conTABuration for PV-energized EV charging station", Energies, vol. 16, no, 6, pp. 2753, 2023.

[3] A. P. Singh, Y. Kumar, Y. Sawle, M. A. Alotaibi, H. Malik, and F. P. G. Márquez, "Development of artificial Intelligence-Based adaptive vehicle-to-grid and grid-to-vehicle controller for electric vehicle charging station", Ain Shams Engineering Journal, vol. 15, no. 10, pp. 102937, 2024.

[4] L. F. Nishimwe H, and S. G. Yoon, "Combined optimal planning and operation of a fast EV-charging station integrated with solar PV and ESS. Energies", vol. 14, no. 11, pp. 3152, 2021.

[5] A. Dukpa, and B. Butrylo, "MILP-based profit maximization of electric vehicle charging station based on solar and EV arrival forecasts", Energies, vol. 15, no. 15, pp. 5760, 2022.

[6] A. K. Karmaker, M. A. Hossain, H. R. Pota, A. Onen, and J. Jung, "Energy management system for hybrid renewable energy-based electric vehicle charging station", IEEE Access, vol. 11, pp. 27793 – 27805, 2023.

[7] U. Datta, A. Kalam, and J. Shi, "Smart control of BESS in PV integrated EV charging station for reducing transformer overloading and providing battery-to-grid service", Journal of Energy Storage, vol. 28, pp. 101224, 2020.

[8] Y. Jang, Z. Sun, S. Ji, C. Lee, D. Jeong, S. Choung, and S. Bae, "Grid-connected inverter for a PV-powered electric vehicle charging station to enhance the stability of a microgrid", Sustainability, vol. 13, no. 24, pp.14022, 2021.

[9] B.K. Santhoshi, K. Mohanasundaram, and L.A Kumar, "ANN-based dynamic control and energy management of inverter and battery in a grid-tied hybrid renewable power system fed through switched Z-source converter", Electrical Engineering, vol. 103, no. 5, pp. 2285 – 2301, 2021.

[10] K. Kouka, A. Masmoudi, A. Abdelkafi, and L. Krichen, "Dynamic energy management of an electric vehicle charging station using photovoltaic power", Sustainable Energy, Grids and Networks, vol. 24, pp. 100402, 2020.

[11] A. A. Mohamed, A. El-Sayed, H. Metwally, and S. I. Selem, "Grid integration of a PV system supporting an EV charging station using Salp Swarm Optimization", Solar Energy, vol. 205, pp. 170-182, 2020.

[12] S. Cheikh-Mohamad, M. Sechilariu, F. Locment, and Y. Krim, "PV-powered electric vehicle charging stations: Preliminary requirements and feasibility conditions", Applied Sciences, vol. 11, no. 4, pp. 1770, 2021.

[13] B. Sun, "A multi-objective optimization model for fast electric vehicle charging stations with wind, PV power and energy storage," Journal of Cleaner Production, vol. 288, pp. 125564, 2021.

[14] Y. Wu, J. Zhang, A. Ravey, D. Chrenko, and A. Miraoui, "Real-time energy management of photovoltaic-assisted

electric vehicle charging station by Markov decision process", Journal of Power Sources, vol. 476, pp. 228504, 2020.

[15] K. P. Joshua, J. Ranga, P. V. Prasad, B. Mallala, M. Rajendiran, and R. Maranan, "Optimized Scheduling of Electric Vehicles Charging in Smart Grid using Deep Learning", In 2024 International Conference on Expert Clouds and Applications (ICOECA), pp. 408 – 412, 2024.

[16] K. S. Kavin, P. Subha Karuvelam, M. Devesh Raj, and M. Sivasubramanian, "A Novel KSK Converter with Machine Learning MPPT for PV Applications", Electric Power Components and Systems, pp. 1– 19, Apr 2024.

[17] A. Raj, and R. P. Praveen, "Highly efficient DC-DC boost converter implemented with improved MPPT algorithm for utility level photovoltaic applications," Ain Shams Engineering Journal, vol. 13, no. 3, pp. 101617, 2022.

[18] H. C. Mohanta, B. T. Geetha, M. S. Alzaidi, I. S. Dhanoa, P. Bhambri, U. Mamodiya, and R. Akwafo, "An Optimized PI Controller-Based SEPIC Converter for Microgrid-Interactive Hybrid Renewable Power Sources", Wireless Communications and Mobile Computing, no. 1, pp. 6574825, 2022.

[19] B. Zhu, J. Liu, Y. Liu, S. Zhi, and Y. Zhao, "A high-reliability SEPIC converter with reconfigurable voltage conversion gain", Energy Reports, vol. 9, pp. 523 – 531, 2023.

[20] J. D. Navamani, A. Geetha, D. Almakhles, A. Lavanya, and J. S. M. Ali, "Modified LUO High Gain DC-DC Converter With Minimal Capacitor Stress for Electric Vehicle Application", in IEEE Access, vol. 9, pp. 122335 – 122350, 2021.

[21] R. Rahimi, S. Habibi, M. Ferdowsi, and P. Shamsi. "Z-source-based high step-up DC–DC converters for photovoltaic applications", IEEE Journal of Emerging and Selected Topics in Power Electronics, vol. 10, no. 4, pp. 4783 – 4796, 2021.

[22] S. F. Faisal, A. R. Beig, and S. Thomas, "Time domain particle swarm optimization of PI controllers for bidirectional VSC HVDC light system", Energies, vol. 13, no. 4, pp. 866, 2020.

[23] J. Gholami, K. K. A. Ghany, and H. M. Zawbaa, "A novel global harmony search algorithm for solving numerical optimizations", Soft Computing, vol. 25, pp. 2837 – 2849, 2021.

[24] A. H. Gana, A. L. Amoo, G. A. Bakare, and A. A. Echo. "Load Frequency Control Strategy for the Nigerian Power System Using Artificial Bee Colony Optimized PI Controller", World Wide Journal of Multidisciplinary Research and Development, vol. 7, no. 6, pp. 25 – 29, 2021.

[25] H. Wang, B. Sheng, Q. Lu, R. Luo, and G. Fu, "A Multi-Objective Cuckoo Search Algorithm Based on the Record Matrix for a Mixed-Model Assembly Line Car-Sequencing Problem", in IEEE Access, vol. 8, pp. 76453 – 76470, 2020.

[26] Kumar, Rahul, Ramani Kannan, Narinderjit Singh Sawaran Singh, Ghulam E. Mustafa Abro, Nirbhay Mathur, and Maveeya Baba. "An efficient design of high step-up switched Z-Source (HS-SZSC) DC-DC converter for grid-connected inverters." Electronics 11, no. 15 (2022): 2440.

[27] M. Saranya, and G. G. Samuel, "Energy management in hybrid photovoltaic–wind system using optimized neural network", Electrical Engineering, vol. 106, no. 1, pp. 475 – 492, 2024.

[28] C. Sathish, I. A. Chidambaram, and M. Manikandan, "Intelligent cascaded adaptive neuro fuzzy interface system controller fed KY converter for hybrid energy-based microgrid applications", Electrical Engineering & Electromechanics, vol. 1, pp. 63 – 70, 2023.

[29] Gopalasami, Ramanathan, Bharatiraja Chokkalingam, and Suresh Muthusamy. "A novel method for hybridization of super lift Luo converter and boost converter for electric vehicle charging applications." Energy Sources, Part A: Recovery, Utilization, and Environmental Effects 45, no. 3 (2023): 8419-8437.

[30] D. T. Prasad, R. Anandhakumar, and P. Balamurugan, "Intelligent MPPT control for SEPIC-Luo converter in grid-tied photovoltaic system", International Journal of Applied, vol. 13, no. 1, pp. 112, 2024.

[31] Z. Wang p. Wang, B. Li, X. Ma, and P. Wang, "A bidirectional DC–DC converter with high voltage conversion ratio and zero ripple current for battery energy storage system", IEEE Trans Power Electron, vol. 36, no. 7, pp. 8012 – 8027, 2020.

[32] H. Bi, Z. Mu, and Y. Chen, "Common grounded wide voltage-gain range DC–DC converter with zero input current ripple and reduced voltage stresses for fuel cell vehicles", IEEE Trans Ind Electron, vol. 70, no. 3, pp. 2607– 2616, 2022.

[33] I. Laoprom, and S. Tunyasrirut, "Design of PI Controller for Voltage Controller of Four-Phase Interleaved Boost Converter Using Particle Swarm Optimization", Journal of Control Science and Engineering 2020, no. 1, pp. 9515160, 2020.

[34] A. H. Sule, A. S. Mokhtar, J. J. B. Jamian, A. Khidrani, and R. M. Larik, "Optimal tuning of proportional integral controller for fixed-speed wind turbine using grey wolf optimizer", International Journal of Electrical and Computer Engineering (IJECE), vol. 10, no. 5, pp. 5251– 5261, 2020.

HOW TO CITE THIS ARTICLE
B. Prabhakar, D. R. Kishore, U. k. Upputuri1, S. S. Suresh, V. Govind, Hybrid Energy System for EV Charging Station Using PV Fed Z-Source Modified Luo Converter and Fuel Cell Integration, AUT J. Elec. Eng., 58(1) (2026) 205-224.

DOI: 10.22060/eej.2025.24379.5697